Molecular Catalysis 564 (2024) 114288

Contents lists available at ScienceDirect

Molecular Catalysis

journal homepage: www.journals.elsevier.com/molecular-catalysis

Research Paper

Two-dimensional Co-based porphyrin metal-organic framework as heterogeneous catalyst for the aerobic oxidation of benzylic hydrocarbon

Andrés Uscategui-Linares [a], Andrea Santiago-Portillo [a], Sergio Navalón [b], Amarajothi Dhakshinamoorthy [b,c], Josep Albero [a,b], Vasile Parvulescu [d], Hermenegildo García [a,*]

[a] Instituto Universitario de Tecnología Química (CSIC-UPV), Universitat Politècnica de València, Av. De los Naranjos, Valencia 46022, Spain
[b] Departamento de Química, Universitat Politècnica de València, C/ Camino de Vera s/n, Valencia 46022, Spain
[c] School of Chemistry, Madurai Kamaraj University, Madurai, Tamil Nadu 625 021, India
[d] Department of Organic Chemistry, Biochemistry and Catalysis, University of Bucharest, B-dul Regina Elisabeta 4-12, Bucharest 030016, Romania

ARTICLE INFO

Keywords:
Aerobic oxidation
Indane
Heterogeneous catalysis
Metal organic frameworks
Two-dimensional

ABSTRACT

The development of heterogeneous catalysts for hydrocarbon oxidation by molecular oxygen as oxidant is an area of increasing interest from academia and chemical industry points of views. Herein, the catalytic activity of two-dimensional (2D) porphyrin metal-organic frameworks (MOFs) constituted by Co^{2+}, Cu^{2+}or Mn^{3+} as transition metal ions coordinated to tetra(4-carboxyphenyl)porphyrin (TCPP) organic ligand as heterogeneous catalysts for the aerobic oxidation of benzylic hydrocarbon oxidation is reported. Selective radical quenching experiments and *in-situ* Raman measurements reveal the formation of superoxide/hydroperoxide and hydroxyl radicals during the catalytic reaction using Co-CoTCPP.

1. Introduction

Aerobic oxidation of hydrocarbons is a very important reaction that is carried out at large industrial scale [1–4]. The main problem of this fundamental reaction is the control of the product selectivity [5,6]. In one general strategy this control on product selectivity can be carried out using a catalyst that drives the reaction towards a few products and minimizes the occurrence of free radical chain reactions taking place in the liquid phase due to the presence of reactive oxygen species (ROS) [7,8].

Among the most important aerobic oxidation catalysts, transition metal complexes are the most widely used [9,10]. Finding inspiration in enzymatic monooxygenase activity [11], transition metal porphyrins in combination with hydrogen peroxide or organic hydroperoxides have been among the most studied oxidation catalysts [12–14]. Cobalt as well as other transition metal-based porphyrins can also promote aerobic oxidations, since they are able to activate molecular oxygen by interacting with it [15–18]. However, the main drawbacks of metal porphyrins as homogeneous catalysts in aerobic oxidations are their deactivation by di- and oligomerization due to the formation of metal-oxo bridges connecting porphyrin units and also the occurrence of free radicals processes that ultimately can lead to degradation of the valuable porphyrin ring [19,20].

As one alternative to the use of soluble or molecular porphyrin complexes, immobilization of the porphyrinic metal complex into a porous host has been a common strategy to develop porphyrin-based heterogeneous catalysts for a wide range of applications [21–23]. Up to now, most of the porous hosts correspond to three dimensional particles in which porphyrins are occluded, as in the case of zeolites and mesoporous aluminosilicates[24,25] or form in part of the lattice as in the case of conventional three dimensional metal-organic frameworks (MOFs) [21]. It appears that immobilization of metal porphyrins in the highly porous open structure of MOFs impedes oligomerization and increases porphyrin stability and by introducing steric hindrance to their attack to the organic macro ring.

Due to their high surface area, large porosity, adequate pore dimensions, the high metal content and the presence of open metal sites [26], MOFs have become among the most widely researched solid catalysts in heterogeneous catalysis [27–32]. In the context of exploiting the potentials of Co-porphyrin based MOFs [32,33], it would be important to determine the catalytic activity of 2D analogues of 3D MOFs as catalysts for aerobic oxidations. 2D MOFs are thin platelets of thickness dimensions[34,35] of a few nanometers that correspond to a countable number of cages in the structure along the vertical direction.

* Corresponding author.
E-mail address: hgarcia@qim.upv.es (H. García).

https://doi.org/10.1016/j.mcat.2024.114288
Received 18 January 2024; Received in revised form 22 May 2024; Accepted 2 June 2024
Available online 8 June 2024

This small thickness allows a much higher exposure of the active sites and also much easier diffusion of reagents and substrates through the material [36]. Moreover, as it has been reported [37], an advantage of 2D MOFs can be their improved structural stability. Therefore, it would be of interest to assess the catalytic activity of 2D MOF porphyrins in general reactions such as aerobic oxidations.

Herein, we report the preparation and characterization of 2D porphyrin-based MOFs and their performance as heterogeneous catalysts in aerobic oxidation of indane as well as diphenylmethane and tetralin. As a probe, we have selected indane since it has only one benzylic position, making simpler product analysis. The oxidation reactions were performed under solvent free conditions using molecular oxygen as oxidizing agent at ambient pressure and temperatures about 140 °C. Essentially complete indane conversion was achieved, Co-porphyrin catalyst being stable and reusable. Hot filtration test indicates that the reaction occurs with the presence of 2D MOF, the free radical chain mechanism contributing to a minor percentage using these 2D MOF catalysts.

2. Experiments and materials

2.1. Materials

The reactants and reagents employed in this study were of analytical or HPLC grade. Cobalt nitrate ($Co(NO_3)_2{\cdot}6H_2O$), zinc nitrate ($Zn(NO_3)_2{\cdot}6H_2O$), copper nitrate ($Cu(NO_3)_2$), *N,N*-dimethylformamide (DMF), nitric acid (HNO_3) and ethanol (EtOH) were purchased from Sigma-Aldrich. Meso-tetra-(4-carboxyphenyl)porphyrin (TCPP) and Mn (III) meso-tetra-(4-carboxyphenyl)porphyrin chloride (Mn(III)TCPP) were purchased from Frontier Scientific®. Cobalt (II) 5,10,15,20-tetra-(4-carboxyphenyl)porphyrin (Co-TCPP) was purchased from PorphyChem.

2.2. Catalysts preparation

2D Co-CoTCPP MOF synthesis. The notation Co-CoTCPP alludes to the two different Co^{2+} ion positions, at the metal nodes of the MOF and complexing the porphyrin macrocycle. $Co(NO_3)_2{\cdot}6H_2O$ (160 mg) and TCPP (145 mg) were dispersed in a solvent mixture containing DMF (28 mL) and EtOH (9 mL). Subsequently, 370 μL of 0.1 M HNO_3 (diluted 1:1 in H_2O/EtOH) was added. The dispersion was sonicated and heated at 80 °C for 24 h. The resulting dark red solid was isolated by filtration and washed with DMF. Finally, the material was further purified with methanol in a Soxhlet extractor and dried under vacuum at 80 °C overnight. For comparison purposes, Zn-ZnTCPP and Cu-CuTCPP were also prepared following exactly the same procedure previously reported for Co-CoTCPP, but replacing $Co(NO_3)_2{\cdot}6H_2O$ by the corresponding metal salt, either $Zn(NO_3)_2{\cdot}6H_2O$ or $Cu(NO_3)_2$ for Zn-ZnTCPP or Cu-CuTCPP, respectively. Co-CoTCPP, Zn-ZnTCPP and Cu-CuTCPP yields were of 57 %, 70 % and 48 %, respectively. The obtained 2D MOFs were used in the catalytic reactions without further treatments.

Syntheses of 2D Co-MnTCPP and Mn-MnTCPP MOFs: $Co(NO_3)_2{\cdot}6H_2O$ (45 mg) or $Mn(CH_3CO_2)_3{\cdot}H_2O$ (27.5 mg) salt, pyrazine (12 mg) and polyvinylpyrrolidone (PVP; 300 mg) were first mixed in a solvent mixture containing DMF (135 mL) and EtOH (45 mL). On the other hand, Mn(III)TCPP (66 mg) was dissolved in a mixture of DMF/EtOH (45 mL/15 mL). Subsequently, the pyrazine and PVP solution was added dropwise to the Mn(III)TCPP solution, sonicated and heated at 80 °C for 24 h. The resulting solids were isolated by filtration and washed with DMF. Finally, the material was further purified with methanol in a Soxhlet extraction system and dried under vacuum at 80 °C overnight.

2.3. Characterization methods

PXRD patterns were acquired with a Shimadzu XRD-7000 diffractometer employing a Cu k_a irradiation source (λ=1.5418 Å) operating at 40 kw and 40 mA. All data acquisition was done at a scanning speed of 10 °/min in the 2θ range 2–90 °. The chemical composition of all samples was determined via combustion chemical analysis employing a CHNS FISONS elemental analyzer. DR UV–VIS spectra were acquired using a Varian Cary 5000 spectrophotometer in the range 200–800 nm. ATR-FTIR spectra were acquired with a Bruker Tensor 27 instrument equipped with a diamond ATR accessory. XPS analyses were recorded through a SPECS spectrometer equipped with a Phoibos 150 MCD-9 detector. The nonmonochromatic X-ray source composed of Al and Mg was operated at 200 W. Before data acquisition, the samples were evacuated at 10^{-9} mbar in the spectrometer prechamber. The measured intensity ratios of the components were obtained from the area of the corresponding peaks after nonlinear Shirley-type background subtraction and corrected by the transition function of the spectrometer. FESEM images were acquired using a ZEISS GeminiSEM 500 electron microscope. The samples were applied directly on the support and subsequently investigated. TEM images were recorded via a JEOL JEM 2100F microscope operating under an accelerating voltage of 200 kV. The samples were uniformly dispersed in an ethanol solution and subsequently dropped casted on carbon coated Ni TEM grids which were allowed to dry at room temperature. AFM measurements were carried out in a Bruker Multimode 8 Nanoscope instrument with a vertical resolution of 3 Å and a horizontal resolution of 5 nm. *In-situ* Raman spectra were recorded at ambient temperature with a 514 nm excitation laser on a Renishaw "*in Via*" spectrophotometer equipped with an Olympus optical microscope and a CCD detector. 20 mg of sample was loaded into a quartz cell adequate for *in-situ* Raman studies. After evacuating the cell ($p < 10$ mbar), Ar, O_2 and Ar were introduced up to a total pressure of ~1 bar. Raman spectra were recorded with a 514 nm laser excitation on a Renishaw Raman Spectrometer ("Refelx") equipped with a CCD detector. The laser power on the sample was 25 mW and a total of 20 acquisitions were taken for each spectrum. A commercial Linkan cell (THMS600) was used for collecting spectra under controlled conditions. Thus, the sample was first subjected to Ar flow (20 mL/min) at 120 °C for 3 h. Afterwards, the gas was changed to O_2 (20 mL/min) at the same temperature. Finally, the O_2 flow was changed to Ar at the same temperature. Oxidation products were confirmed by comparing the retention times and mass spectra of the reaction products with authentic commercial samples using gas chromatography coupled with mass spectrometer (GC-MS) 5977C GC/MSD Agilent instrument.

2.4. Catalytic reaction procedure

In a typical catalytic experiment, previously activated solid catalyst (5 mg) at 140 °C under vacuum for 6 h placed in a round-bottom flask (25 mL) was charged with 2.5 mL of freshly distilled indane free of stabilizers. This slurry was placed on a hot plate and maintained at 140 °C, while purging with an oxygen flow without touching the liquid from an inflated balloon under constant magnetic stirring. Aliquots were periodically taken at different time intervals to monitor the reaction mixture. A known volume of the aliquot was diluted in a known volume of a solution of acetonitrile containing a known amount of nitrobenzene as external standard. During sampling at different time intervals, the round bottom flask was sealed with septum and the aliquots were taken through a syringe. These samples were injected into Agilent gas chromatography (GC) using a flame ionization detector. The products were confirmed by co-injecting with authentic commercial samples of the oxidation products . Further, the oxidation products were also confirmed by GC–MS, comparing retention times and mass spectra with commercial samples as reference. These procedures were repeated in those experiments to determine the influence of radical quenchers by performing the above reaction with 20 mol % of *p*-benzoquinone or dimethyl sulfoxide respect to the substrate. On the other hand, hot filtration tests were performed as indicated above, but the solid catalyst was removed by filtration with the nylon filter with syringe after initiation of the reaction at above 25 % conversion. This reaction mixture without the solid

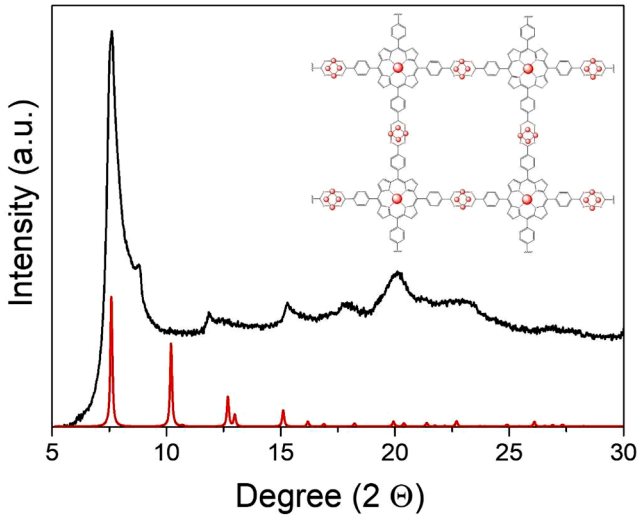

Fig. 1. PXRD pattern of Co-CoTCPP (black) and simulated single crystal pattern (red). Inset shows a scheme of the proposed structure.

catalyst was allowed to react further under the same conditions in the absence of any solid until the end of the reaction. Later, the organic phase was analysed for the presence of metals by extracting it with 30 mL of 3 M aqueous HNO_3 solution and the aqueous solution submitted to chemical analysis using an ICP-AES instrument (Varian 715-ES, CA, USA).

3. Results and discussion

3.1. Catalysts preparation and characterization

The 2D-based MOFs under study have been prepared based on previous reported procedure[26] with some modifications, and the experimental details can be found in the in experimental section. The synthesis was performed with the solvents of DMF containing ethanol in a 3-to-1 proportion acidified with aqueous nitric acid. The synthesis was carried out at 80 °C for 24 h. Besides 2D MOFs of a single metal (Co, Zn, Cu and Mn), other analogous material having Co at the MOF nodes and Mn at the porphyrin ring was also prepared (see experimental procedures) for comparison purposes (vide infra). Fig. 1 shows the powder XRD pattern of Co-CoTCPP (Fig. S1 shows an extended diffraction pattern acquired up to 90 º) and the simulated diffraction pattern for a Co-CoTCPP single crystal model. This is in good agreement with previous reports [38,39], where the main diffraction peak at a 2θ value of 7.6° has been attributed to the 110 facet [40]. The differences between the experimental and simulated XRD patterns at long angles has been previously observed in the literature and attributed to the stacking of the Co-CoTCPP sheets in comparison to the single crystal model. [40] Furthermore, no peaks that could be attributable to cobalt oxides, including the most intense ones at 37 and 42 º, were recorded. The XRD patterns of Zn-ZnTCPP, Cu-CuTCPP, Mn-MnTCPP and Co-MnTCPP are also presented in Fig. S2. These XRD patterns are also very similar to those reported in the literature [41-43].

Co-CoTCPP MOF morphology corresponds to an ultrathin 2D layered material, as it can be observed from the TEM and AFM images in Fig. 2, and TEM and HRFESEM images in Fig. S3. The TEM images (Figs. 2a and b) show that the solid is constituted by ultrathin 2D platelets of several microns lateral size, exhibiting the presence of wrinkles, indicative of the material flexibility, similarly to other ultrathin 2D materials, such as graphene. Measurements in AFM images of Co-CoTCPP (Fig. 2c) show that this 2D MOF has an average thickness of 5.42 ± 0.55 nm. This small thickness can also be visualized in TEM images at high resolution that shows the border of the sheets (Fig. 2b). TEM images of Zn-ZnTCPP and Cu-CuTCPP MOFs also confirm their 2D morphology (see Fig. S4).

The metal content in the different 2D MOFs was determined by elemental ICP-OES measurements, and a summary of the obtained values is presented in Table S1. The Co content in Co-CoTCPP was 13.35 wt.%, while Zn, Cu and Mn contents were 17.90, 17.65 and 10.00 wt.% for Zn-ZnTCPP, Cu-CuTCPP and Mn-MnTCPP, respectively.

Further investigation of the chemical composition and coordination sphere of the elements of the synthesized 2D Co-CoTCPP MOF was carried out by XPS (Fig. S5). The high-resolution XPS C 1 s peak on Co-CoTCPP shows three components centered at 284.5, 285.4 and 288.6 eV, attributable to sp^2 C atoms, C atoms bonded to N and O—C = O bonds, respectively. The high-resolution XPS O 1 s spectrum peak fits also with three components at 529.2, 531.6 and 533 eV binding energy that can be assigned to Co-O, C = O and C—OH bonds, respectively. The N 1 s spectrum shows two main components at 398.2 and 399.5 eV, ascribed to pyridinic N atoms and amine moieties (or other sp^3 C atoms bonded to

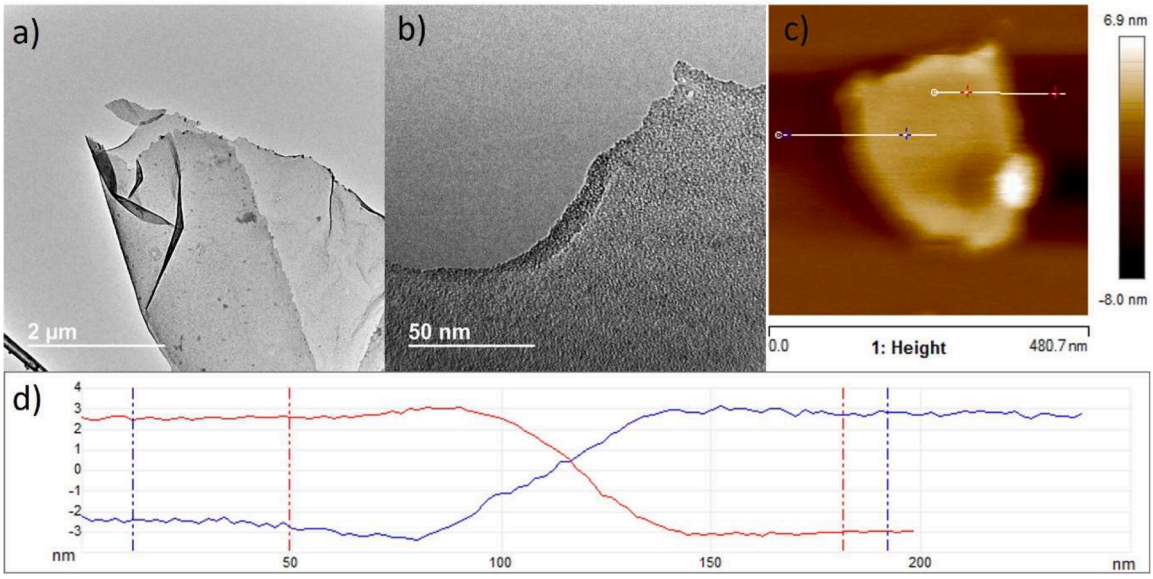

Fig. 2. TEM (a and b) and AFM images of Co-CoTCPP MOF (c). The thickness of Co-CoTCPP nanosheets across white lines indicated in panel c has been measured in the AFM vertical profile with sub-nanometric resolution (d).

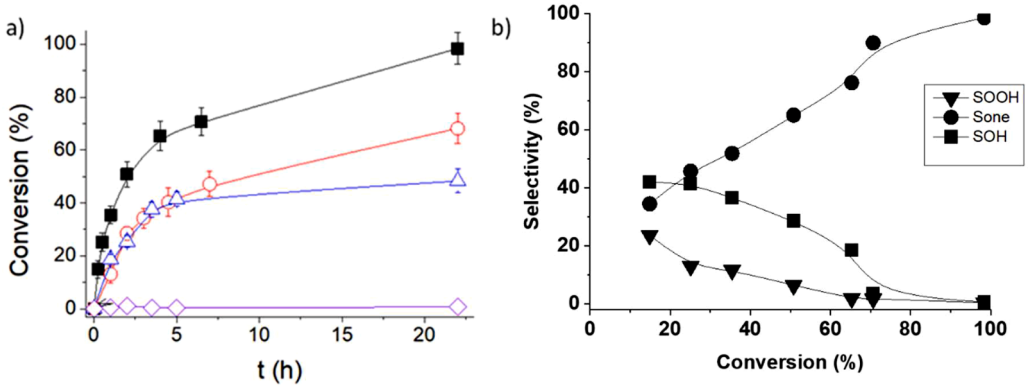

Fig. 3. (a) Aerobic oxidation of indane with various 2D MOFs. Legend: 2D MOFs having as porphyrin metal Co (■), Cu (○), Zn (Δ) and Mn (◊). (b) Selectivity-conversion plot for the aerobic oxidation of indane using Co-TCPP MOF. Indanone (●, Sone) indanol (▲, Sol), indane hydroperoxide (▼, SOOH)). Reaction conditions: Catalyst (5 mg) activated under vacuum overnight at 140 ºC, 20 mmol indane, 140 ºC, under oxygen atmosphere through balloon. Note: the error bars correspond to the standard deviation of two independent catalytic test repetitions.

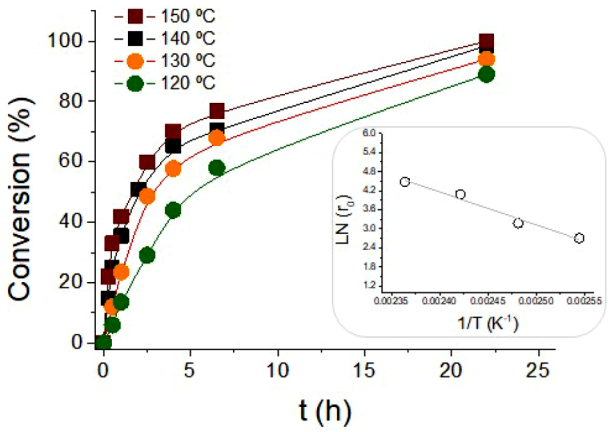

Fig. 4. Influence of reaction temperature on the aerobic oxidation of indane using Co-CoTCPP as catalyst. Reaction conditions: Co-CoTCPP (5 mg) activated under vacuum overnight at 140 ºC, 20 mmol indane, temperature as mentioned in the figure, under oxygen atmosphere through balloon.

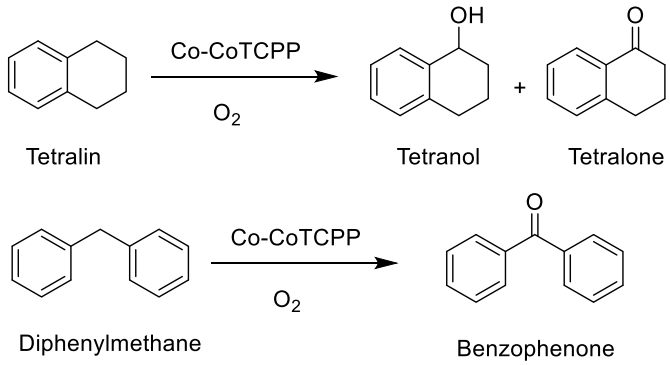

Scheme 1. Aerobic oxidation of tetralin and diphenylmethane using Co-CoTCPP MOF as a catalyst.

N) [44]. It is worth noticing that the typical component related to free amino groups at 401.7 eV has not been observed, and, therefore, we can assume that -NH moieties are not present and that all the N atoms are coordinated Co. Finally, the high-resolution Co $2p_{3/2}$ spectrum shows two components at 780.2 and 781.9 eV, attributed to Co^{2+} coordinated to O and Co in the porphyrin complex, respectively [44–46]. These data confirm not only the presence of the Co-porphyrin complex but also Co^{2+} forming the nodes in the 2D MOF.

Further confirmation of TCPP metalation in the different 2D MOFs is provided by the diffuse reflectance (DR…) UV–Vis spectra presented as Fig. S6. As can be seen there, the typical four Q bands in the free base porphyrin (TCPP) in the visible region cannot be observed, and, instead, two main bands characteristic of the different metals coordinated in porphyrin ring are recorded [47].

3.2. Catalytic activity

After ascertaining the structural integrity and characteristic features of the as-synthesised 2D MOFs, the catalytic activity of these materials was tested in the aerobic oxidation of indane at 140 ºC under solvent-less conditions. Among the series of the four monometallic 2D MOFs, the activity of Co-CoTCPP was significantly higher compared to the analogous Cu, Zn and Mn 2D MOFs (Fig. 3a). Co-CoTCPP not only provides high conversion of indane, but this Co MOF also exhibits higher initial reaction rate than that of Zn-ZnTCPP, Cu-CuTCPP, Mn-MnTCPP, and higher selectivity to indanol (4 %) and indanone (92 %) after 22 h at 140 °C is observed (Figs. S7-S8). It should be noted that the presence of hydroperoxides, dimeric compounds and other products is highly undesirable in the reaction. Notably, the observed catalytic results are in good agreement with literature reports, where Co is the preferred metal to efficiently promote aerobic oxidation reactions [33]. The temporal product evolution shown in Fig. 3b shows that indanone is a primary and secondary stable product, while indanol and indanyl hydroperoxide are primary but unstable products, becoming transformed into indanone.

The influence of the reaction temperature on the catalytic of Co-CoTCPP MOF for the aerobic oxidation of indane was also studied. Fig. 4 shows that both initial reaction rate and conversion at 22 h gradually increases as a function of the temperature. In addition, Fig. 4b shows that the catalytic data follows the Arrhenius plot with an estimated apparent activation energy of 86 kJ/mol. Furthermore, the catalytic performance of Co-CoTCPP MOF was tested with two other benzylic hydrocarbons, namely tetralin and diphenylmethane under identical conditions used for the aerobic oxidation of indane. For instance, Co-CoTCPP MOF showed 15 % conversion of tetralin with the selectivity to tetranol (23 %) and tetranone (77 %) after 22 h (Scheme 1, Figs. S9-S10). On other hand, the aerobic oxidation of diphenylmethane using Co-CoTCPP MOF catalyst afforded 10 % conversion with complete selectivity to benzophenone as product (Scheme 1, Fig. S11). These results indicate that Co-CoTCPP MOF can also promote the aerobic oxidation of other benzylic substrates. It is noteworthy to mention that the conversion of benzylic hydrocarbon depends on various factors, like kinetic diameter of the substrate, its electronic nature, and effective intimacy between the active site in Co-CoTCPP and the substrate.

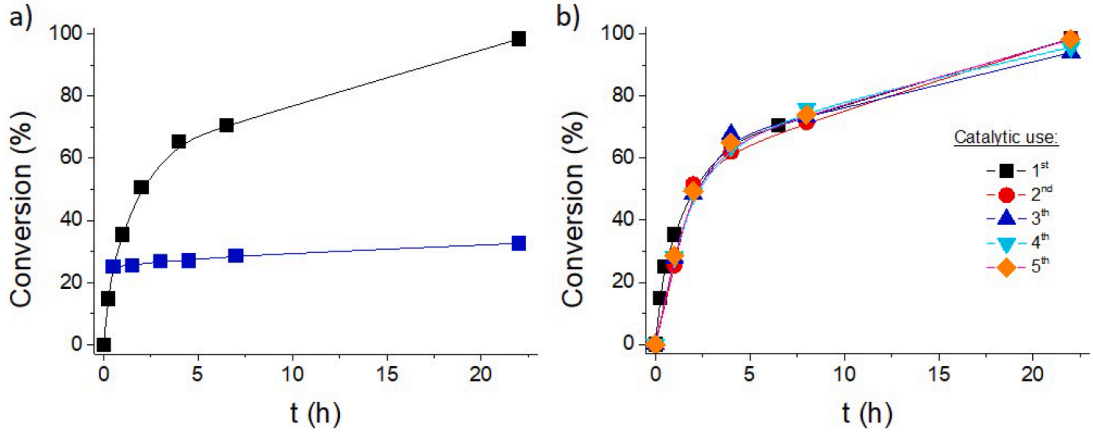

Fig. 5. (a) Hot filtration test and (b) reusability tests for aerobic oxidation of indane using Co-TCPP as solid catalyst. Reaction conditions: Co-CoTCPP (5 mg) activated under vacuum overnight at 140 ºC, 20 mmol indane, 140 ºC, under oxygen atmosphere through balloon.

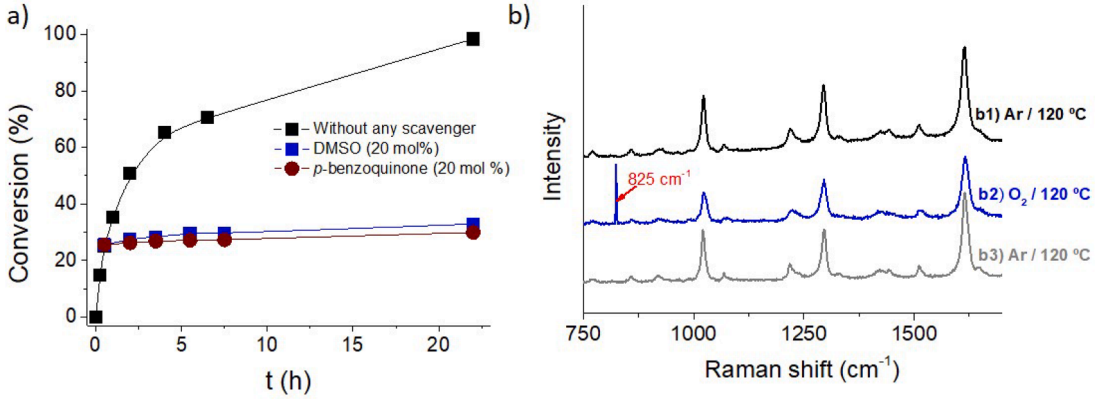

Fig. 6. a) Influence of radical quenchers (indicated in the plot) on the conversion of indane with Co-CoTCPP catalyst; b) Raman spectra recorded for Co-CoTCPP treated at 120 °C for 30 min consecutively with an Ar flow (b1), with an O_2 flow (b2) and an Ar flow (b3). The peak labelled at 825 cm^{-1} in spectra b2 is attributed to the O_2 bound to Co-CoTCPP.

One important issue that is relevant in heterogeneous catalysis is to prove the stability of the catalyst under the optimized reaction conditions. In this aspect, heterogeneity and reusability tests were performed with Co-CoTCPP under the optimal reaction conditions and the observed results are presented in Fig. 5a. Aerobic oxidation of indane was initiated in the presence of Co-CoTCPP and the solid catalyst was removed at the conversion around 25 % and the reaction mixture at this point in the absence of solid was allowed to continue the reaction under the same conditions until 24 h. Time conversion plots with and without solid catalysts indicate that the reaction completely stops upon removal of the solid, thus suggesting the heterogeneity of the process under these conditions. Furthermore, this hot filtration test also proves the role of Co-CoTCPP as a catalyst and not as a radical initiator generating some free reactive oxygen species in solution that could continue indane oxidation through a long chain radical reaction. In addition, leaching of Co ions from Co-CoTCPP in the hot filtration test was quantified by inductively coupled plasma analysis, observing undetectable amounts. This analysis further confirms the stability of Co-CoTCPP under the present experimental conditions.

Then, reusability experiments were performed, and the observed catalytic data indicate that the solid is reusable at least up to five cycles with no decrease in the initial reaction rate or in the final conversion (Fig. 5b). These results clearly prove the catalytic stability of Co-CoTCPP under reaction conditions. Further confirmation of the Co-CoTCPP stability obtained by characterization of the five times used material by TEM (Fig. S12a) and chemical analysis of the liquid phases as well as the resulting solid show a negligible loss of Co in the material. XPS analysis after reusability experiments have been also carried out, and the results are presented in Fig. S12 b. As can be seen there, the Co 2p 3/2 XPS peak of Co-CoTCPP clearly presents a positive shift of 0.6 eV. This is indicating a partial oxidation of the Co sites during the reaction. Furthermore, powder XRD of the fresh and five times used solid was compared, observing that no structural deterioration are apparent after the use of the sample in five consecutive oxidation reaction (Fig. S13).

3.3. *Reaction mechanism*

Initially, selective radical quenching experiments and *in-situ* Raman measurements were carried out to characterize the possible formation of ROS during the aerobic oxidation. For this purpose, *p*-benzoquinone and DMSO were employed as selective superoxide/hydroperoxide and hydroxyl radical scavengers, respectively. Fig. 6a shows that once the reaction has started (30 % conversion) addition of any of the two oxygen-centered radical scavengers almost completely inhibits the reaction. The fact that the reaction has started, and the conversion is notable ensures that a sufficient stationary build-up of the ROS cocktail has taken place. Based on previous reports about O_2 activation by heterogeneous catalysts including MOFs [48,49], these observations can be interpreted considering that superoxide/hydroperoxide radicals are the primary species formed that ultimately leads to the formation of hydroxyl radicals as secondary species. The coincidence of the quenching with the two scavengers indicates that the main role in the indane oxidation is played

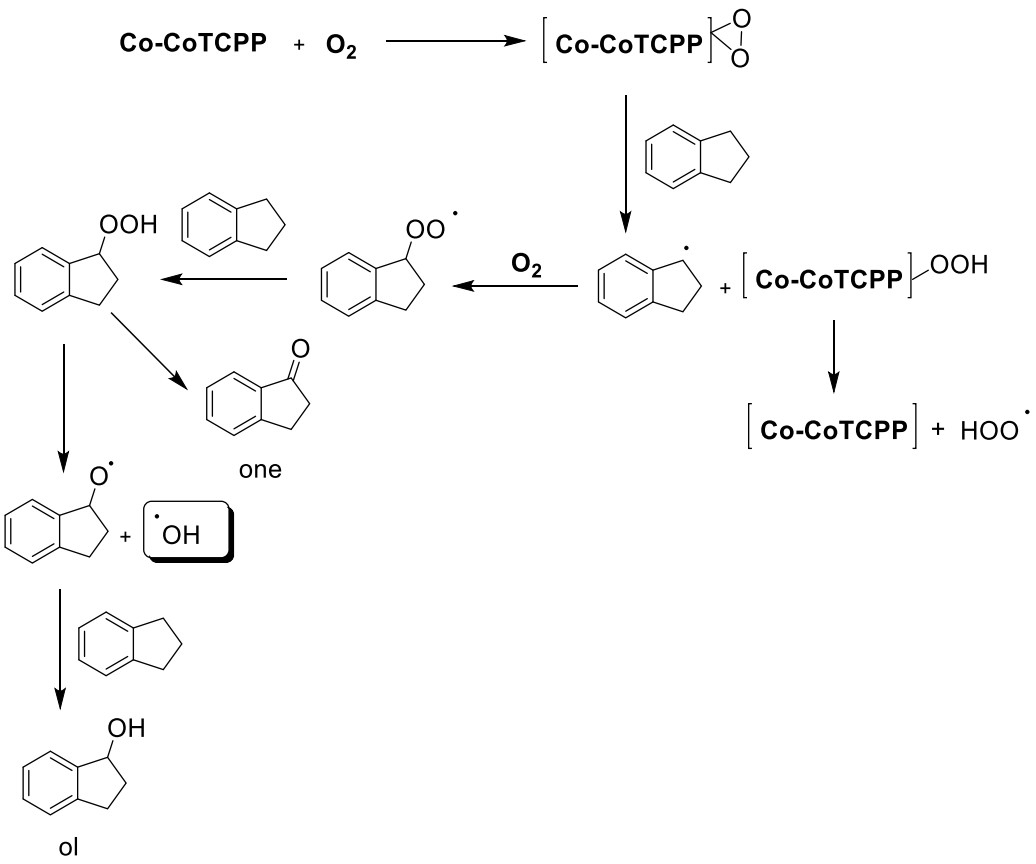

Scheme 2. Proposed mechanism for the aerobic oxidation of indane catalyzed by Co-CoTCPP solid catalyst.

by hydroxyl radicals, since otherwise, DMSO would not have intercepted the intrinsic activity of superoxide/hydroperoxyl and some progress in indane conversion should have been observed in this case. Scheme 2 summarizes the reaction mechanism for the aerobic oxidation of indane catalysed by Co-CoTCPP solid catalyst.

To further understand the role of cobalt species to activate molecular O_2 towards the formation of ROS, *in-situ* Raman spectroscopic measurements were carried out using Co-CoTCPP. For this purpose, the solid catalyst was submitted to prior activation at 120 °C under Ar flow for 30 min to remove adsorbed water and other species. Subsequently, the system was purged with O_2 at 120 °C for additional 30 min trying to simulate the reaction temperature. As it can be seen in Fig. 6b, this treatment results in the formation a new Raman peak at 825 cm^{-1} that can be attributed to the formation of cobalt peroxo intermediate [50, 51]. Later, the sample was submitted again to an Ar flow at 120 °C for 30 min, observing the complete disappearance of the band at 825 cm^{-1} indicating the reversible decomposition of the cobalt peroxo species formed within the Co-CoTCPP MOF. The other vibration bands in the Raman spectrum characteristic of Co-CoTCPP remain unaltered during the *in-situ* treatments. These results would agree with the formation of initial cobalt peroxo species that under the reaction conditions can lead to the formation of hydroperoxyl and hydroxyl radicals as evidenced by selective radical quenching experiments.

As commented before, Co-CoTCPP MOF have two possible active sites, the Co^{2+} coordinated in the porphyrin ring or/and the Co^{2+} clusters in the MOF nodes. To elucidate which Co ions are the actual active sites, a commercial Co-TCPP metal complex and Co-MnTCPP have been used as catalysts. The powder XRD and DR UV–Vis spectra of Co-TCPP metal complex is presented in Fig. S14. Co-TCPP is characterized by the presence of Co^{2+} coordinated in the porphyrin ring. In the case of the Co-MnTCPP MOF the Mn^{3+} ions are coordinated to the porphyrin ring, while Co^{2+} are present in the metal nodes of the solid. It is worth reminding that the catalytic activity of 2D Mn-MnTCPP MOF had been already tested and shows negligible activity for this reaction

Table 1
Data of indane oxidation catalysed with the porphyrin MOFs employed in this study.

Catalyst	Con. (%)	Selectivity (%)			Remarks
		indanol	indanone	1-indanyl hydroperoxide	
Co-CoTCPP	100	4	92	4	Co^{2+} at the nodal positions or Co^{2+}complexed within the porphyrin ring acts synergistically to promote the aerobic oxidation efficiently.
Co-TCPP metal complex	72	9	59	32	The activity is lower compared to Co-CoTCPP, probably due to the lack of Co^{2+}ions in the metal nodal positions.
Co-MnTCPP	77	6	66	28	The activity is lower compared to Co-CoTCPP due to the lack of Co^{2+}ions in the porphyrin ring.
Mn-CoTCPP	46	9	62	29	The activity is lower compared to Co-CoTCPP due to the lack of Co^{2+}ions in the nodal positions.
Mn-TCPP	–	–	–		No activation of O_2
Mn-MnTCPP	–	–	–		No activation of O_2 either by Mn^{3+} nodal position or by Mn^{3+} coordinated with porphyrin carboxylates.

Table 2
Comparison of the activity of Co-CoTCPP with other reported solid catalysts for the oxidation of indane.

Catalyst	Reaction conditions	Conv. (%)	Sel. (%)[a]	Remarks	Refs.
MIL-101 (Cr)	75 mg of catalyst, 20 mmol indane, 120 °C, O_2, 30 h.	98	64, 8	MIL-101 can generate carbon centered radicals in the presence of molecular oxygen	[52]
Fe(BTC)	25mg of Fe(BTC), 1 mmol indane, 20 mg of tetrabutylammonium bromide, 2 mL acetonitrile, O_2, 80 °C, 24h.	18	3, 97	Fe(BTC) and tetrabutylammonium bromide promote the oxidation through radical mechanism.	[53]
Co-MIL-173(Zr)	2 mg catalyst, 20 mmol indane, 120 °C, O_2, 30 h, 18h	100	95[b]	Co-MIL-173(Zr) behaves as a heme-like heterogeneous catalyst activating O_2 in the aerobic oxidation of indane	[54]
Co-CoTCPP	5 mg of catalyst, 20 mmol indane, 140 °C, O_2, 22 h.	100	92,4	Co peroxo complex is formed by reaction with O_2 and Co^{2+} in porphyrin linker as well as in the metal node plays crucial role.	This work

[a] Selectivity refers to the percentage values for indanone and indanol, respectively.
[b] The original data report combined selectivity of indanol+indanone.

(Fig. 3a), and therefore, any activity in Co-MnTCPP should be reasonably attributed to the Co nodes. Co-TCPP metal complex and Co-MnTCPP MOF showed 72 % and 77 % conversions after 22 h, respectively. Further, Co-TCPP metal complex afforded 9 % and 59 % indanol and indanone selectivity, while Co-MnTCPP MOF exhibit 6 % and 66 % selectivity to indanol and indanone, respectively after 22 h. On the other hand, the activity of Mn-CoTCPP was tested for the aerobic oxidation of indane under identical conditions, observing 46 % conversion with 9 % and 62 % selectivity to indanol and indanone, respectively. Interestingly, no indane oxidation was observed for Mn-TCPP complex, this result being in agreement with previously commented data on the activity of 2D Mn-MnTCPP MOF. These data are presented in Table 1. The activity of both samples indicates that both types of Co^{2+} ions, either at the MOF nodes coordinated with carboxylate groups (Co-CoTCPP) or the porphyrin Co central ion (Co-TCPP) can promote the aerobic oxidation. It should be noted, however, that the selectivity to the ol/one products was lower than in the case of Co-MnTCPP, suggesting that there could be an additional synergetic effect in the case of Co-CoTCPP.

Furthermore, the activity of Co-CoTCPP in the aerobic oxidation of indane was also compared with other literature reports. As commented earlier in the introduction, the activity of 3D MOFs has been extensively studied in heterogeneous catalysis compared to their analogous 2D MOFs. In this aspect, some of us have already reported the activity of MIL-101 in the aerobic oxidation of indane [52]. MIL-101(Cr) exhibited 87 % selectivity at 30 % conversion, while the activity of MIL-101(Fe) was 71 % selectivity at 30 % conversion. The enhanced selectivity towards ol/one products with MIL-101(Cr) was due to the preferential adsorption of indane within the pore system, thus facilitating higher density of substrates near to the active sites. In another precedent, Fe(BTC) was employed as a solid catalyst to promote the aerobic oxidation of indane without using any initiators under mild reaction conditions [53]. The catalytic data showed 18 % conversion of indane with 97 % selectivity to indanol at 80 °C in acetonitrile as solvent using tetrabutylammonium bromide as a cocatalyst. Although the above mentioned three MOFs are 3D particles with different structural properties, different active sites and the experimental reaction conditions could not be exactly identical, the present solid, Co-CoTCPP shows better activity and selectivity to ol/one compared to these three 3D solids. This result illustrates the advantage of having accessible catalytic sites exposed on a 2D surface as compared to 3D porous materials in which reagent diffusion and site accessibility can decrease the reaction rate [36]. Table 2 summarizes the catalytic activity for indane oxidation, comparing the performance of Co-CoTCPP with other literature reports. It should be noted that comparison of the catalytic activity of Co-CoTCPP with other catalysts is complicated due to the differences in the reaction conditions, including reaction temperature, time, solvent and oxidant nature.

4. Conclusions

The 2D metal porphyrin MOFs of only a few nm thicknesses appear as promising heterogeneous catalysts for the aerobic oxidation of hydrocarbons. Using indane as probe in the absence of solvent, it has been possible to achieve for Co-CoTCPP complete conversion using O_2 at atmospheric pressure as terminal oxidizing reagent. The process exhibits a high selectivity to indanone at complete conversion. Other 2D porphyrinic MOF analogues of Zn, Cu and Mn exhibit poorer performance. The 2D Co MOF is catalytically stable and reusable, hot filtration test showing the absence of significant Co leaching and the fact that the reaction is not promoted by free ROS in solution through a long propagation chain reaction mechanism. An apparent activation energy of 86 kJ/mol was estimated from the influence of the reaction temperature on the initial reaction rate. Quenching studies indicate that the reaction is mostly promoted by hydroxyl radical generated through superoxide/hydroperoxide intermediate. *In-situ* Raman spectroscopy upon heating in the presence of O_2 at 120 °C reveals the appearance of a new band at 825 cm^{-1} that can be attributed to the Co peroxo complex formed by reaction of molecular oxygen and Co^{2+} porphyrin. Using models of Co^{2+} at the nodal positions or complexed within the porphyrin macro-ring indicate that both types of Co^{2+} ions can promote the aerobic oxidation. The present results illustrate the potential that 2D MOFs have as heterogeneous catalysts of organic reactions with enhanced performance compared to 3D MOFs, provided that the reaction conditions are compatible with MOF stability.

CRediT authorship contribution statement

Andrés Uscategui-Linares: Investigation. **Andrea Santiago-Portillo:** Investigation. **Sergio Navalón:** Formal analysis, Data curation. **Amarajothi Dhakshinamoorthy:** Investigation, Formal analysis, Data curation. **Josep Albero:** Supervision, Data curation. **Vasile Parvulescu:** Writing – original draft, Conceptualization. **Hermenegildo García:** Writing – review & editing, Conceptualization.

Declaration of competing interest

The authors declare that they have no known competing financial interests or personal relationships that could have appeared to influence the work reported in this paper.

Data availability

Data will be made available on request.

Acknowledgements

Financial support the Spanish Ministry of Science and Innovation

(Severo Ochoa CEX2021–1230-S financed support by MCIN/AEI/10.13039/501100011033), and Generalitat Valenciana (Prometeu 2021–038 and MFA-2022–023 financed by European Union-Next Generation EU, through the Conselleria de Innovación, Universidades, Ciencia y Sociedad Digital) are gratefully acknowledged. J.A. thanks the Spanish Ministry of Science and Innovation for a Ramon y Cajal research associate contract (RYC2021–031006-I financed support by MCIN/AEI/10.13039/501100011033 and by European Union/NextGenerationEU/PRTR). S.N. thanks the support of grant PID2021-123856OBI00 funded by MICIU/AEI/10.13039/501100011033 and by ERDF A way of making Europe. A.D. is beneficiary of a grant María Zambrano in Universitat Politècnica de València within the framework of the grants for the retraining in the Spanish university system (Spanish Ministry of Universities, financed by the European Union, NextGeneration EU).

Supplementary materials

Supplementary material associated with this article can be found, in the online version, at doi:10.1016/j.mcat.2024.114288.

References

[1] Y. Ishii, S. Sakaguchi, T. Iwahama, Innovation of hydrocarbon oxidation with molecular oxygen and related reactions, Adv. Synth. Catal. 343 (2001) 393–427.
[2] H.R.B. Derek, D. Doller, The selective functionalization of saturated hydrocarbons: Gif chemistry, Acc. Chem. Res. 25 (1992) 504–512.
[3] H. Sterckx, B. Morel, B.U.W. Maes, Catalytic aerobic oxidation of C(sp^3)−H, bonds, Angew. Chem. Int. Ed. 58 (2019) 7946–7970.
[4] Y. Ishii, S. Sakaguchi, Recent progress in aerobic oxidation of hydrocarbons by N-hydroxyimides, Catal. Today 117 (2006) 105–113.
[5] M. Caruso, S. Navalón, M. Cametti, A. Dhakshinamoorthy, C. Punta, H. García, Challenges and opportunities for N-hydroxyphthalimide supported over heterogeneous solids for aerobic oxidations, Coord. Chem. Rev. 486 (2023) 215141.
[6] R. Raja, J.M. Thomas, Catalyst design strategies for controlling reactions in microporous and mesoporous molecular-sieves, J. Mol. Catal. A; Chem. 181 (2002) 3–14.
[7] J. Long, H. Liu, S. Wu, S. Liao, Y. Li, Selective oxidation of saturated hydrocarbons using Au–Pd alloy nanoparticles supported on metal–organic frameworks, ACS Catal. 3 (2013) 647–654.
[8] S. Pradhan, R. Lloyd, J.K. Bartley, D. Bethell, S. Golunski, R.L. Jenkins, G. J. Hutchings, Multi-functionality of Ga/ZSM-5 catalysts during anaerobic and aerobic aromatisation of n-decane, Chem. Sci. 3 (2012) 2958–2964.
[9] M. Navarro, A. Escobar, V.R. Landaeta, G. Visbal, F. Lopez-Linares, M.L. Luis, A. Fuentes, Catalytic oxidation of tetralin by biologically active copper and palladium complexes, Appl. Catal. A: Gen. 363 (2009) 27–31.
[10] R. Neumann, A.M. Khenkin, Molecular oxygen and oxidation catalysis by phosphovanadomolybdates, Chem. Commun. (2006) 2529–2538.
[11] J. Jiang, R. Luo, X. Zhou, F. Wang, H. Ji, Metalloporphyrin-mediated aerobic oxidation of hydrocarbons in cumene: Co-substrate specificity and mechanistic consideration, Mol. Catal. 440 (2017) 36–42.
[12] P.D. Harvey, Porphyrin-based metal- and covalent-organic frameworks as heterogeneous nanosized photocatalysts in organic synthesis, J. Mater. Chem. C 9 (2021) 16885–16910.
[13] Y. Yang, G. Li, X. Mao, Y. She, Selective aerobic oxidation of 4-ethylnitrobenzene to 4-nitroacetophenone promoted by metalloporphyrins, Org. Proc. Res. Dev. 23 (2019) 1078–1086.
[14] C.-C. Guo, X.-Q. Liu, Y. Liu, Q. Liu, M.-F. Chu, X.-B. Zhang, Studies of simple μ-oxo-bisiron(III)porphyrin as catalyst of cyclohexane oxidation with air in absence of cocatalysts or coreductants, J. Mol. Catal. A; Chem. 192 (2003) 289–294.
[15] J.T. Groves, T.E. Nemo, Aliphatic hydroxylation catalyzed by iron porphyrin complexes, J. Am. Chem. Soc. 105 (1983) 6243–6248.
[16] D. Mansuy, Activation of alkanes: the biomimetic approach, Coord. Chem. Rev. 125 (1993) 129–141.
[17] M.W. Grinstaff, M.G. Hill, J.A. Labinger, H.B. Gray, Mechanism of catalytic oxygenation of alkanes by halogenated iron porphyrins, Science 264 (1994) 1311–1313.
[18] J.E. Lyons, P.E. Ellis, H.K. Myers, Halogenated metalloporphyrin complexes as catalysts for selective reactions of acyclic alkanes with molecular oxygen, J. Catal. 155 (1995) 59–73.
[19] M. Dashteh, Spotlight: Porphyrin-based catalysts, Iran, J. Catal. 10 (2020) 247–252.
[20] U.S. Agarwalla, Catalytic oxyfunctionalization of saturated hydrocarbons by non-heme oxo-bridged diiron(III) complexes: role of acetic acid on oxidation reaction, Transition Metal, Chem 45 (2020) 583–588.
[21] M. Zhao, S. Ou, C.-D. Wu, Porous metal–organic frameworks for heterogeneous biomimetic catalysis, Acc. Chem. Res. 47 (2014) 1199–1207.
[22] M. Silva, M.E. Azenha, M.M. Pereira, H.D. Burrows, M. Sarakha, C. Forano, M. F. Ribeiro, A. Fernandes, Immobilization of halogenated porphyrins and their copper complexes in MCM-41: Environmentally friendly photocatalysts for the degradation of pesticides, Appl. Catal. B. Environ. 100 (2010) 1–9.
[23] M. Madadi, R. Rahimi, Zeolite-immobilized Mn(III), Fe(III) and Co(III) complexes with 5,10,15,20-tetra(4-methoxyphenyl)porphyrin as heterogeneous catalysts for the epoxidation of (R)-(+)-limonene: synthesis, characterization and catalytic activity, React. Kinet. Mech. Catal. 107 (2012) 215–229.
[24] V. Radha Rani, M. Radha Kishan, S.J. Kulkarni, K.V. Raghavan, Immobilization of metalloporphyrin complexes in molecular sieves and their catalytic activity, Catal. Commun. 6 (2005) 531–538.
[25] J. Haber, K. Pamin, J. Połtowicz, Cationic metalloporphyrins and other macrocyclic compounds in zeolite matrix as catalysts for oxidation with dioxygen, J. Mol. Catal. A; Chem. 224 (2004) 153–159.
[26] E.-Y. Choi, C.A. Wray, C. Hu, W. Choe, Highly tunable metal–organic frameworks with open metal centers, CrystEngComm 11 (2009) 553–555.
[27] H. Li, M. Eddaoudi, M. O'Keeffe, O.M. Yaghi, Design and synthesis of an exceptionally stable and highly porous metal-organic framework, Nature 402 (1999) 276–279.
[28] C.-D. Wu, A. Hu, L. Zhang, W. Lin, A homochiral porous metal−organic framework for highly enantioselective heterogeneous asymmetric catalysis, J. Am. Chem. Soc. 127 (2005) 8940–8941.
[29] D. Farrusseng, S. Aguado, C. Pinel, Metal–organic frameworks: Opportunities for catalysis, Angew. Chem. Int. Ed. 48 (2009) 7502–7513.
[30] A. Dhakshinamoorthy, A.M. Asiri, H. García, Metal–organic frameworks as multifunctional solid catalysts, Trends Chem 2 (2020) 454–466.
[31] S. Biswas, M. Maes, A. Dhakshinamoorthy, M. Feyand, D.E. De Vos, H. Garcia, N. Stock, Fuel purification, Lewis acid and aerobic oxidation catalysis performed by a microporous Co-BTT (BTT^{3-} = 1,3,5-benzenetristetrazolate) framework having coordinatively unsaturated sites, J. Mater. Chem. 22 (2012) 10200–10209.
[32] A. Dhakshinamoorthy, A. López-Francés, S. Navalon, H. Garcia, Porous metal organic frameworks as multifunctional catalysts for cyclohexane oxidation, ChemCatChem 14 (2022) e202201036.
[33] A. Dhakshinamoorthy, E.M. Lanzuela, S. Navalon, H. Garcia, Cobalt-based metal organic frameworks as solids catalysts for oxidation reactions, Catalysts 11 (2021) 1–26.
[34] M. Ko, L. Mendecki, K.A. Mirica, Conductive two-dimensional metal–organic frameworks as multifunctional materials, Chem. Commun. 54 (2018) 7873–7891.
[35] G. Chakraborty, I.-H. Park, R. Medishetty, J.J. Vittal, Two-dimensional metal-organic framework materials: Synthesis, structures, properties and applications, Chem. Rev. 121 (2021) 3751–3891.
[36] A. Dhakshinamoorthy, A.M. Asiri, H. Garcia, 2D metal–organic frameworks as multifunctional materials in heterogeneous catalysis and electro/photocatalysis, Adv. Mater. 31 (2019) 1900617.
[37] Y. Xue, G. Zhao, R. Yang, F. Chu, J. Chen, L. Wang, X. Huang, 2D metal–organic framework-based materials for electrocatalytic, photocatalytic and thermocatalytic applications, Nanoscale 13 (2021) 3911–3936.
[38] N. Kornienko, Y. Zhao, C.S. Kley, C. Zhu, D. Kim, S. Lin, C.J. Chang, O.M. Yaghi, P. Yang, Metal–organic frameworks for electrocatalytic reduction of carbon dioxide, J. Am. Chem. Soc. 137 (2015) 14129–14135.
[39] S.R. Ahrenholtz, C.C. Epley, A.J. Morris, Solvothermal preparation of an electrocatalytic metalloporphyrin MOF thin film and its redox hopping charge-transfer mechanism, J. Am. Chem. Soc. 136 (2014) 2464–2472.
[40] R. Makiura, K. Tsuchiyama, O. Sakata, Self-assembly of highly crystalline two-dimensional MOF sheets on liquid surfaces, CrystEngComm 13 (2011) 5538–5541.
[41] M. Zhao, Y. Wang, Q. Ma, Y. Huang, X. Zhang, J. Ping, Z. Zhang, Q. Lu, Y. Yu, H. Xu, Y. Zhao, H. Zhang, Ultrathin 2D metal–organic framework nanosheets, Adv. Mater. 27 (2015) 7372–7378.
[42] D.T. Lee, J.D. Jamir, G.W. Peterson, G.N. Parsons, Water-stable chemical-protective textiles via euhedral surface-oriented 2D Cu–TCPP metal-organic frameworks, Small 15 (2019) 1805133.
[43] N. Sharma, S.S. Dhankhar, C.M. Nagaraja, A Mn (II)-porphyrin based metal-organic framework (MOF) for visible-light-assisted cycloaddition of carbon dioxide with epoxides, Microporous Mesoporous Mater 280 (2019) 372–378.
[44] W. Wu, Q. Zhang, X. Wang, C. Han, X. Shao, Y. Wang, J. Liu, Z. Li, X. Lu, M. Wu, Enhancing selective photooxidation through Co–Nx-doped carbon materials as singlet oxygen photosensitizers, ACS Catal 7 (2017) 7267–7273.
[45] K.B.K.B. Yatsimirskii, V.V. Nemoskalenko, V.G. Aleshin, Y.I. Bratushko, E. P. Moiseenko, X-ray photoelectron spectra of mixed oxygenated cobalt(II)-amino acid-imidazole complexes, Chem. Phys. Lett. 52 (1977) 481–484.
[46] Y. Chen, S. Jie, C. Yang, Z. Liu, Active and efficient Co-N/C catalysts derived from cobalt porphyrin for selective oxidation of alkylaromatics, Appl. Surf. Sci. 419 (2017) 98–106.
[47] F. Espitia-Almeida, C. Díaz-Uribe, W. Vallejo, O. Peña, D. Gómez-Camargo, A.R. R. Bohórquez, X. Zarate, E. Schott, Photodynamic effect of 5,10,15,20-tetrakis(4-carboxyphenyl)porphyrin and (Zn^{2+} and Sn^{4+}) derivatives against Leishmania spp in the promastigote stage: experimental and DFT study, Chem. Papers 75 (2021) 4817–4829.
[48] A. Dhakshinamoorthy, A.M. Asiri, J.R. Herance, H. Garcia, Metal organic frameworks as solid promoters for aerobic autoxidations, Catal. Today 306 (2018) 2–8.
[49] A. Dhakshinamoorthy, M. Alvaro, H. Garcia, Metal–organic frameworks as heterogeneous catalysts for oxidation reactions, Catal. Sci. Technol. 1 (2011) 856–867.
[50] A. Gómez-Paricio, A. Santiago-Portillo, S. Navalón, P. Concepción, M. Alvaro, H. Garcia, MIL-101 promotes the efficient aerobic oxidative desulfurization of dibenzothiophenes, Green Chem 18 (2016) 508–515.

[51] B. Shin, K.D. Sutherlin, T. Ohta, T. Ogura, E.I. Solomon, J. Cho, Reactivity of a cobalt(III)–hydroperoxo complex in electrophilic reactions, Inorg. Chem. 55 (2016) 12391–12399.
[52] A. Santiago-Portillo, S. Navalón, F.G. Cirujano, F.X. Llabrés i Xamena, M. Alvaro, H. Garcia, MIL-101 as reusable solid catalyst for autoxidation of benzylic hydrocarbons in the absence of additional oxidizing reagents, ACS Catal 5 (2015) 3216–3224.
[53] N. Nagarjun, A. Dhakshinamoorthy, Aerobic oxidation of benzylic hydrocarbons by iron-based metal organic framework as solid heterogeneous catalyst, ChemistrySelect 3 (2018) 12155–12162.
[54] G. Mouchaham, B. Abeykoon, M. Gimenez-Marques, S. Navalon, A. Santiago-Portillo, M. Affram, N. Guillou, C. Martineau, H. Garcia, A. Fateeva, T. Devic, Adaptability of the metal (III, IV) 1, 2, 3-trioxobenzene rod secondary building unit for the production of chemically stable and catalytically active MOFs, Chem. Commun. 53 (2017) 7661–7664.